AN ABSTRACT OF THE THESIS OF

Ibrahem S. Elayeb for the degree of Master of Science in Civil Engineering presented on June 13, 2016.

Title: An Experimental Study on Violent Geysers in Vertical Shafts

Abstract approved: _____

Arturo S. Leon

A Geyser in a stormwater (SW) and combined sewer system (CSS) is an oscillatory and violent release of a mixture of air and water through vertical shafts. Violent geysers are highly destructive. In the case of combined sewer systems, many municipalities operate their systems at a fraction of their maximum capacity to avoid transients and geysers. Operating CSSs at a fraction of their capacity means that these systems are not fully utilized and hence, combined sewer overflows (CSOs) occur more often than they should. These overflows contain not only stormwater but also untreated human and industrial waste, toxic materials, and debris. The U.S. Environmental Protection Agency estimates that in 31 states and the District of Columbia, 772 combined sewer systems with more than 9,000 CSO outfalls annually discharge about 850 billion gallons of untreated wastewater and stormwater. Geysers have been studied numerically and experimentally for over three decades. Even though geysers were studied for a relatively

long time, their violent behavior was neither reproduced experimentally nor numerically. The motivation of this thesis is to present the results of an experimental study that for the first time produced violent geysers (few consecutive eruptions with heights that may exceed 30m) that resemble those observed in the field. This experimental study also included tests of a retrofitting method for minimizing geyser intensity in terms of height and eruption velocity. The retrofitting consists of a simple diameter reduction (e.g., orifice) at the bottom of the dropshaft. The dimensionless eruption height and velocity were found to have a good fit with the power forms obtained in the dimensional analysis. The eruption height and velocity were found to increase with the dimensionless air mass flow rate and the ratio between dropshaft height and dropshaft diameter. Results indicate that the eruption height and velocity decrease with a decrease in orifice diameter (e.g., lower air mass flow rate). For the experimental conditions considered in the present study, the proposed retrofitting method was found to be an effective strategy for minimizing the intensity of violent geysers where a geyser eruption is nearly eliminated when the ratio between orifice diameter and dropshaft diameter is about 1/8.

An Experimental Study on Violent Geysers in Vertical Shafts

by

Ibrahem S. Elayeb

A THESIS

submitted to

Oregon State University

in partial fulfillment of
the requirements for the
degree of

Master of Science

Presented June 13, 2016
Commencement June 2017

Master of Science thesis of Ibrahem S. Elayeb presented on June 13, 2016.

APPROVED:

Major Professor, representing Civil Engineering

Head of the School of Civil and Construction Engineering

Dean of the Graduate School

I understand that my thesis will become part of the permanent collection of Oregon State University libraries. My signature below authorizes release of my thesis to any reader upon request.

Ibrahem S. Elayeb, Author

ACKNOWLEDGEMENTS

First and foremost, I would like to express my gratitude to my advisor, Dr. Arturo S. Leon, for his support, guidance, and encouragement throughout my graduate studies. His technical advice was essential to the completion of this thesis and has taught me innumerable lessons in hydraulics and academic research in general.

I would like to thank all of my family and friends for their support during my graduate studies. Through all of their encouragement, moral support, and edible support, I have been enabled to complete this goal. I am especially grateful to my mom, for her love and understanding during the past couple of years. Her support and late-night calls.

Finally, I would also like to thank all of the professors and graduate students with whom I've had the pleasure of meeting and working with at Oregon State University.

TABLE OF CONTENTS

LIST OF FIGURES

LIST OF TABLES

Chapter 1: Introduction

Although stormwater (SW) and combined sewer systems (CSSs) are unique in their geometry, in general, these systems consist of near-horizontal tunnels, which serve as storage, and vertical shafts, which serve as ventilation columns or as access points for maintenance. During intense rainfall events, SW and CSSs may undergo a rapid filling, leading to highly dynamic conditions and air entrapment (e.g., [Hamam and McCorquodale, 1982], [Vasconcelos, 2005], [Leon et al., 2010], [Lewis, 2011], [Wright et al., 2011]). When the entrapped air arrives at vertical shafts (dropshafts), a high frequency oscillatory release of a mixture of gas (e.g., air) and liquid may occur. This event is known as a geyser. The oscillating jet of gas-liquid mixture may reach a height of the order of a few to tens of meters above ground level. Violent geysers are highly destructive. A video of a geyser that occurred at Interstate 35W (Minnesota) on 07/03/1999 can be seen at `http://www.youtube.com/watch?v=4aQySL0sKys`. Three snapshots of this video are shown in Fig. 1.1. Combined sewer systems (CSSs) are usually operated at a fraction of their full capacity to avoid transients and geysers (e.g., [Leon et al., 2006]). Operating CSSs at a fraction of their full capacity means that these systems are not fully utilized and hence, combined sewer overflows (CSOs) occur more often than they should (e.g., [Leon, 2006]). The U.S. Environmental Protection Agency (EPA) estimates that in 31 states and

the District of Columbia, 772 combined sewer systems with more than 9,000 CSO outfalls discharge about 850 billion gallons of untreated wastewater and stormwater annually ([EPA, 2004]). Combined sewer overflows contain not only storm water but also untreated human and industrial waste, toxic materials, and debris, which have a negative impact on water quality and recreational uses in local waterways.

Figure 1.1: Snapshots of a geyser produced on Interstate 35W (Minnesota, 07/03/1999) `https://www.youtube.com/watch?v=Jp7zLbBs0Rc`

Geysers have been studied over three decades in terms of water phase only or air-water interaction (e.g., [Hamam and McCorquodale, 1982], [Guo and Song, 1991], [Lewis, 2011]). These studies include laboratory experiments and numerical modeling. Various of these studies focused on the analysis of dynamic flow conditions under which surges and geysers could occur. [Hamam and McCorquodale, 1982], [Vasconcelos, 2005] and [Lewis, 2011] studied the mechanisms through which air is entrapped in horizontal tunnels. Furthermore, a number of laboratory experiments (e.g., [Vasconcelos, 2005], [Lewis, 2011]) have been conducted to produce geysers, however none of these experiments resembled the characteristics of violent geysers observed in actual systems.

Field studies on geysers are rarely documented due to its seldom occurrence. A series of geysers at Interstate 35W (Minnesota) were documented, however the sampling rate of the data was inadequate for a detailed analysis ([Wright et al., 2011]). According to [Wright et al., 2011], pressure and velocity data were recorded every five minutes using two pressure transducers and a velocity probe. These authors pointed out that the maximum pressure head recorded was far below the pressure required to lift the water to the ground level. Also, pressure data indicated no inertial oscillations. These authors concluded that surging in the tunnel system is not associated to the occurrence of geysers.

Even though geysers were studied for a relatively long time, their violent behaviour was neither reproduced experimentally nor numerically. The motivation of this paper is to present the results of an experimental study that, for the first time, produced violent geysers in a laboratory setting (e.g., a few consecutive violent eruptions within a time frame of a couple of seconds with heights that may exceed 30 m) that resemble those observed in the field. As an example, Fig. 1.2 shows three snapshots of a geyser produced in one of our laboratory experiments.

Figure 1.2: Snapshots of a geyser produced in one of our laboratory experiments

This research aims to experimentally study explosive geysers which will be produced in the laboratory and propose a retrofitting method to minimize geyser intensity. This thesis is divided as follows. First, a dimensional analysis for the geyser experiments is briefly presented. Second, the experimental setup is briefly described. Third, the experimental results are presented and discussed. Finally, the key results are summarized in the conclusion.

Chapter 2: Material and Methods

2.1 Geyser Dimensional Analysis

The geyser height (h_g) [m] is dominated by the physical constants of the liquid (e.g., water) and gas (e.g., air), namely, the kinematic viscosity (ν) [m^2/s], the density (ρ) [kg/m^3] and the surface tension (σ) [N/m]. The first two variables should be considered for the liquid and gas phases, however as indicated in [Pfister and Chanson, 2014], the gas constants are of minor significance. In addition, the geyser height is influenced by the gas mass flow rate ($\dot{M}$) [kg/s], the gravitational acceleration (g) [m/s^2], the diameter of the dropshaft (D) [m] and the dropshaft height (H) [m]. Thus, the geyser height, in a two-phase air-water flow, is a function of the following variables, where the subindex w indicates the water liquid.

$$h_g = f(H, g, D, \dot{M}, \rho_w, \sigma, \nu_w) \tag{2.1}$$

There are eight variables in Eq. (2.1) and three basic dimensions (mass, length and time). Thus, five dimensionless terms can be obtained, which are shown in Eq. (2.2)

$$\frac{h_g}{D} = \phi\left(\frac{\dot{M}}{\rho_w\sqrt{gD^5}}, \frac{H}{D}, \frac{(\sqrt{gD})D}{\nu_w}, \frac{\rho_w(\sqrt{gD})^2 D}{\sigma}\right) \tag{2.2}$$

The fourth and fifth dimensionless terms are equivalent to the Reynolds number (*Re*) and the Weber number (*We*), respectively, where the term $\sqrt{gD}$ can be thought as a characteristic velocity in the vertical pipe. Literature in the area of two-phase flows suggests that for high-speed air-water flows, scale effects related to air concentration are small when $Re > 3{\times}10^5$ and $We^{0.5} > 170$ (e.g., [Pfister and Chanson, 2014]). Because air concentration is highly related to geyser occurrence (water droplets entrained into gas slugs), the above limits for *Re* and *We* may be applicable to geyser flows as well. For the set of experiments of the present paper, the minimum geyser velocity is about 5 m/s (e.g., characteristic velocity), D = 0.15 m, $\nu \approx 10^{-6}$ m^2/s, and $\sigma \approx 73 \times 10^{-3}$ N/m. For these values, *Re* and $We^{0.5}$ are 7.5×10^5 and 227, respectively, which are larger than the above limiting values. Thus, the relevant dimensionless terms for geyser height and velocity can be reduced to:

$$\frac{h_g}{D} = \phi\left(\frac{\dot{M}}{\rho_w\sqrt{gD^5}}, \frac{H}{D}\right) \tag{2.3}$$

To represent h_g/D as a function of the second and third dimensionless terms in Eq. (2.3), it is assumed that h_g/D obeys the following power form

$$\frac{h_g}{D} = \alpha 1\left(\frac{\dot{M}}{\rho_w\sqrt{gD^5}}\right)^{\alpha 2}\left(\frac{H}{D}\right)^{\alpha 3} \tag{2.4}$$

where $\alpha 1$, $\alpha 2$ and $\alpha 3$ are empirical constants. According to the ballistic equation, the geyser velocity (w) and geyser height (h_g) are related by $w = \sqrt{2gh_g}$. Thus, a dimensional geyser

velocity, as a function of the same aforementioned variables, can be defined as

$$\frac{w}{\sqrt{gD}} = \beta 1 \left(\frac{\dot{M}}{\rho_w \sqrt{gD^5}} \right)^{\beta 2} \left(\frac{H}{D} \right)^{\beta 3} \tag{2.5}$$

where $\beta 1 = \sqrt{2\alpha 1}$, $\beta 2 = \alpha 2/2$ and $\beta 3 = \alpha 3/2$.

2.2 Laboratory Experiments

2.2.1 Experimental Setup

The apparatus for this experimental study is shown schematically in Fig. 2.1. The horizontal and vertical pipe consisted of clear PVC schedule 80 with an internal diameter of $6''$(0.152 m). The upstream tank, which was made of fiberglass, has a total volume of 1.7 m^3 and a maximum operating pressure of 150 psi (absolute). The upstream tank is connected to the horizontal pipe through a $6''$ gate valve, which controls the flow from the head tank. Another ball valve with $3''$ (0.0762 m) diameter was installed at the end of the downstream pipe to drain the water from the system.

For the retrofitting method, an orifice plate was installed at the bottom of the vertical pipe. The retrofitting consists of a simple diameter reduction (e.g., orifice) at the bottom of the drop-shaft. Three orifice diameters were tested, namely $3''$, $1.5''$ and $0.75''$. The perspective and plan views of the orifice retrofitting are shown in Figure (2.2).

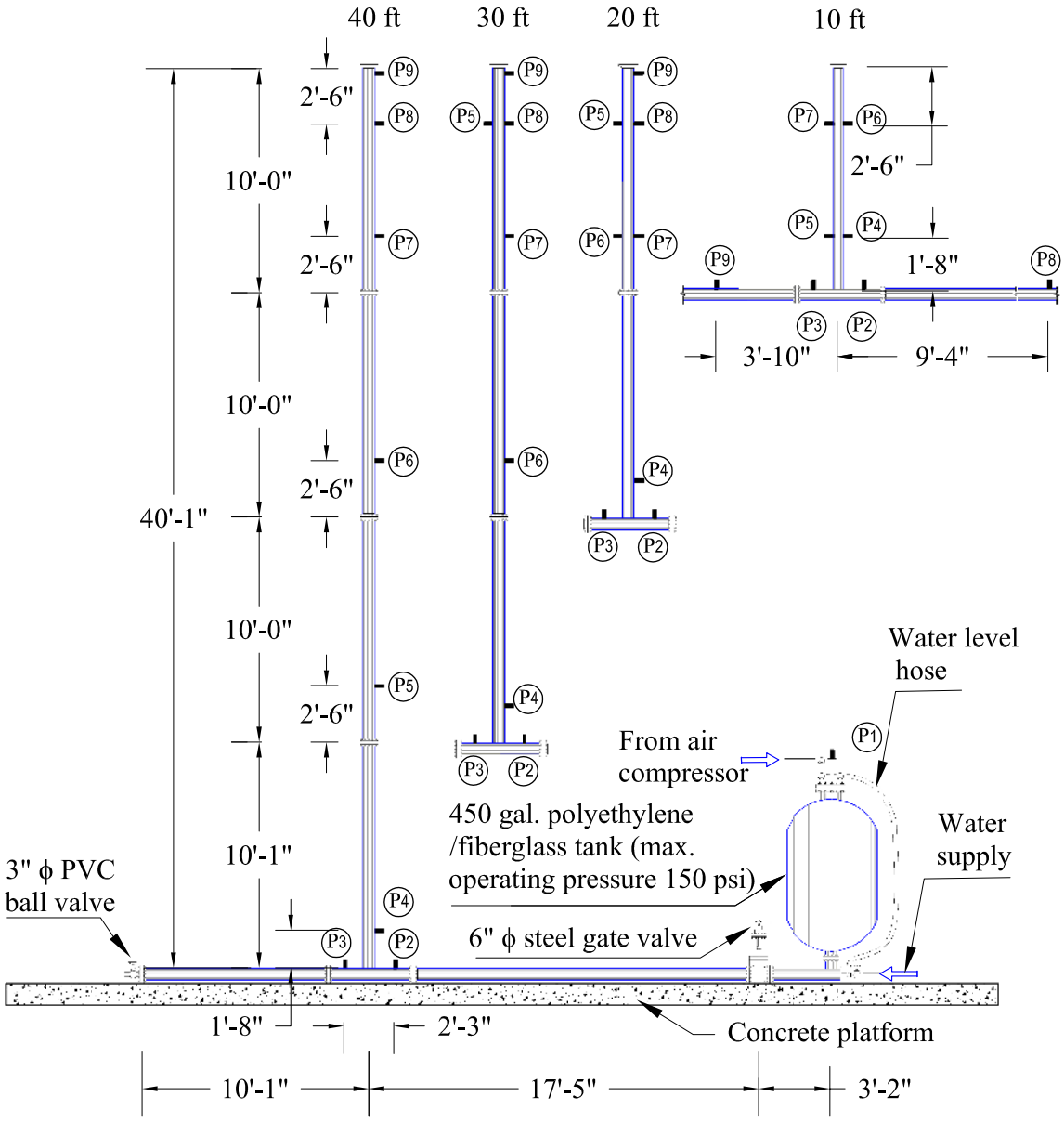

Figure 2.1: Sketch of experimental setup (Not To Scale)

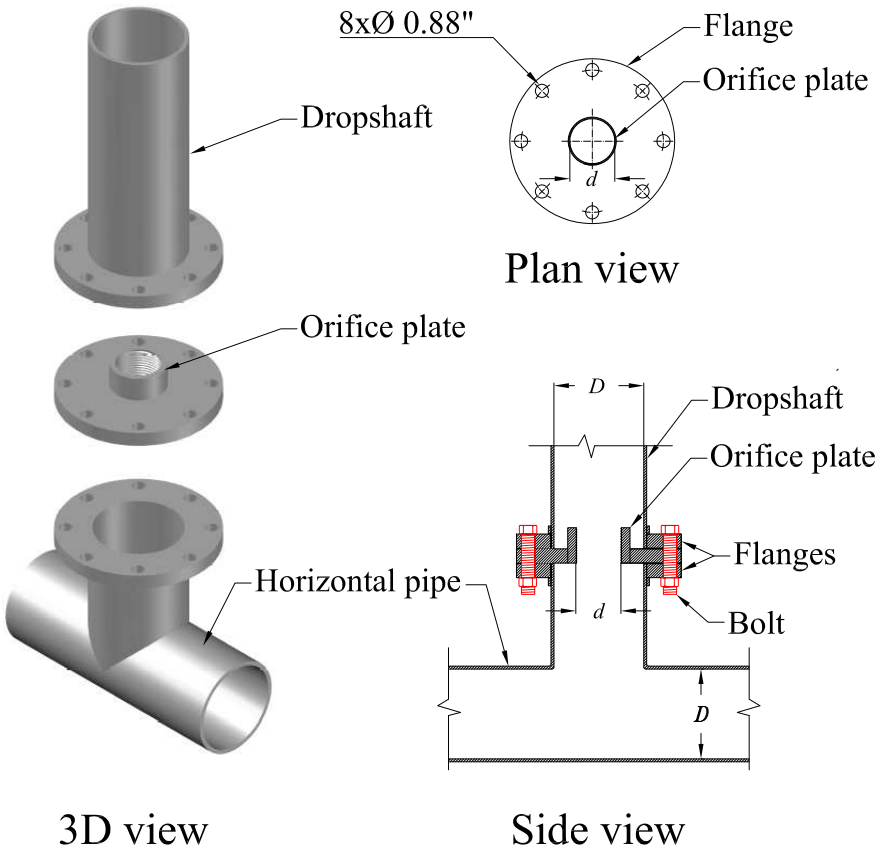

Figure 2.2: Sketch of Retrofitting system (Not To Scale)

24 experimental configurations (see Table 2.1) were created by varying three parameters for each diameter. The first parameter was the initial air pressure in the upstream tank, which values ranged from 34 to 78 psi (absolute). The initial pressures were obtained by trial and error to make sure that the upstream gate is fully opened before the geysering. The second parameter was the dropshaft height (3, 6, 9 and 12 m), which is the same as the initial water height. The third parameter was the water volume (205 and 254 gallons). The experiments with 205 gallons

(0.7760 m^3) are denoted as *Series 1* (S1) experiments and those with 254 gallons (0.9615 m^3) are denoted as *Series 2* (S2) experiments. Every experimental run was repeated at least three times to ensure repeatability of the experimental results. This resulted in at least 72 experiments (24×3) for each diameter. The total number of experiments performed were 372.

Table 2.1: Initial absolute air pressures (psi) in the upstream tank for the 24 experimental configurations

Dropshaft length (m)	S1: 205 gal			S2: 254 gal		
12	60	61	62	74	76	78
9	51	52	53	64	66	68
6	43	44	45	53	55	57
3	34	35	37	44	45	47

2.2.2 Measurement Equipment

The measurement equipment used in this study includes:

1. Nine piezo-resistive pressure transducers (UNIK 5000) (absolute pressure range from 2.5 to 63.3 m H_2O, frequency response of 3.5 KHz, and accuracy of 0.04% full-scale). The

location of the pressure transducers for the four dropshaft heights is shown in Fig. 2.1. An example of pressure heads recorded with the nine sensors for a geyser experiment is shown in Fig. 2.3.

2. An ultrasonic flow meter (FDT-40), which was installed near the downstream end of the horizontal pipe (maximum velocity 12 m/s and accuracy of 1% of reading).

3. A high-speed video camera (Edgetronic) was used to record the geyser height over the dropshaft and track air pocket motion in the horizontal and vertical pipe.

4. Two National Instruments data acquisition board NI 6321 with eight differential channels and sampling rate up to 250 kHz integrated with LabVIEW were used for data acquisition.

5. Two thermometers (measurement range from -3 to 40 °C with an accuracy of 0.2 °C) were used to measure water and air temperature at the beginning of each experiment.

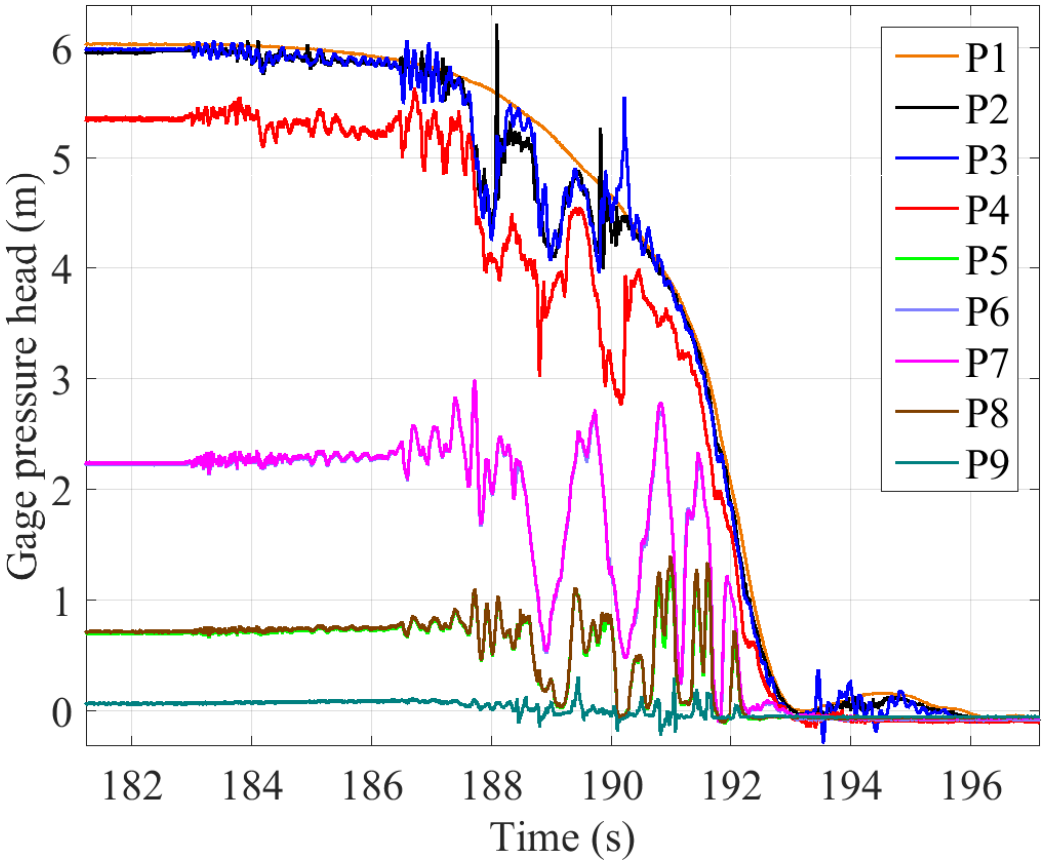

Figure 2.3: An example of pressure heads recorded with the nine sensors for a geyser experiment

2.2.3 Experimental Procedure

The experimental procedure was as follows:

1. The upstream tank is filled with water until the level corresponding to the volume of 205 (*Series 1*) or 254 (*Series 2*) gallons.

2. The top of the upstream tank is pressurized with air to the pressure specified in Table 2.1. This pressure is controlled with pressure sensor 1 located in the upstream tank (P1 in Fig. 2.1).

3. After the tank is pressurized, the data acquisition system (DAQ) starts to acquire data.

4. Once the DAQ is acquiring data, the upstream gate valve is fully opened. Having the upstream gate valve fully opened before the geysering avoids water level oscillations in the dropshaft before the geysering occurs.

5. A short time ($\sim$ 5 to 60 seconds) after the gate is fully opened, an air pocket will enter the dropshaft and produce geyser eruptions. The mechanisms that lead to violent geysers in vertical shafts are described in [Leon, 2016b].

6. After the geyser eruptions are terminated, the data recording is stopped.

2.2.4 Data Summary

A summary of the data for both series of experiments are shown in Table 2.2 to 2.5. In this table, T_w is water temperature, T_a is air temperature, P_a is initial air pressure in the tank, V_w is initial water volume upstream of the gate valve, V_a is initial air volume in the tank, and t is the geysering time (time from the entry of the air pocket to dropshat until the ending of geyser eruptions). The geysering time was obtained from the measured pressure traces by identifying

the beginning and ending of pressure fluctuations. As an example, the measured pressure traces in Figure 2.3 show that the most upstream sensor in the horizonal pipe (sensor P2) started to register the pressure signal of the air pocket at about 183 s and it ended at about 193 s. The pressure signal after 193 s corresponds to the period after the depressurization of the dropshaft. The geyser velocity was obtained using the ballistic equation given by $w = (2gh_g)^{1/2}$, where h_g is the geyser height, which is obtained from the video recordings. The average air mass flow rate was obtained as the initial air mass divided by the geysering time.

Table 2.2: Geyser data for NR experiments (d = 6″, $d/D = 1$, (No retrofitting))

	S1 (V_w = 0.772 m^3, V_a = 0.918 m^3)					*S2* (V_w = 0.961 m^3, V_a = 0.729 m^3)				
H	T_w	T_a	P_a	t	h_g	T_w	T_a	P_a	t	h_g
(m)	(°C)	(°C)	(psi)	(s)	(m)	(°C)	(°C)	(psi)	(s)	(m)
3	18.5	17.2	34	47.5	3.11	20.5	22.2	44	13.6	4.85
3	18.7	17.4	34	26.6	3.09	20.6	22.3	44	14.6	4.26
3	18.8	17.8	34	31.8	3.37	20.6	22.2	44	14.8	2.53
3	18.9	18.0	34	30.1	3.37	20.8	22.4	44	20.3	5.86
3	18.9	18.3	34	32.2	3.66	21.0	22.3	44	16.4	5.43
3	19.2	18.8	35	17.9	4.91	21.1	22.5	45	25.1	1.63
3	19.2	19.5	35	18.9	5.81	21.1	22.5	45	15.9	4.58
3	19.4	20.1	35	14.6	4.67	21.2	22.4	45	30.3	2.94

3	19.5	20.7	35	32.9	3.39	21.1	22.6	45	25.9	2.66
3	19.5	21.1	35	15.8	5.57	21.3	22.7	45	17.5	1.84
3	19.1	15.2	37	26.9	5.72	21.2	22.8	47	19.5	5.70
3	19.2	15.8	37	15.9	5.46	21.4	22.7	47	30.5	5.59
3	19.2	16.7	37	18.3	5.63	21.5	22.8	47	13.3	4.70
3	19.4	17.5	37	18.2	5.49	21.4	22.9	47	28.1	5.41
3	19.3	18.3	37	14.2	4.68	21.5	23.0	47	21.1	6.16
6	18.6	17.2	43	13.0	10.26	18.5	16.1	53	17.4	9.08
6	18.4	17.0	43	13.1	13.24	18.7	16.8	53	16.7	9.51
6	18.1	16.5	43	13.3	11.51	18.8	17.1	53	16.7	9.65
6	18.0	15.5	43	13.1	10.83	18.8	17.0	53	19.0	10.85
6	17.6	14.4	43	12.7	13.33	19.0	17.8	53	18.2	9.16
6	17.7	13.1	44	10.4	11.56	18.7	15.6	55	13.7	16.22
6	17.8	13.3	44	11.7	10.37	18.9	16.3	55	13.0	8.33
6	17.8	13.5	44	10.6	14.38	19.0	16.9	55	15.9	11.28
6	18.2	13.8	44	11.1	17.55	19.1	17.7	55	13.5	14.08
6	18.1	14.1	44	15.3	13.36	19.3	18.3	55	13.6	8.99
6	18.2	14.2	45	9.6	12.87	19.5	21.1	57	10.1	13.67
6	18.2	14.4	45	10.1	10.22	19.7	21.4	57	9.3	15.32
6	18.3	14.7	45	10.0	13.76	19.8	21.9	57	11.0	12.83

6	18.4	14.8	45	9.0	12.65	20.0	22.4	57	10.3	14.95
6	18.4	15.0	45	10.0	11.30	20.3	23.2	57	10.4	19.90
9	21.1	21.2	51	15.1	19.78	22.6	22.8	64	16.9	17.96
9	21.3	21.0	51	15.5	21.23	22.9	23.7	64	18.4	23.63
9	21.4	20.7	51	17.8	20.50	23.3	24.5	64	15.9	19.76
9	21.6	20.3	51	17.5	19.01	23.7	25.9	64	14.9	24.90
9	21.7	20.0	51	15.5	20.74	24.0	26.8	64	16.6	24.54
9	18.5	13.9	52	13.1	22.06	21.7	16.1	66	12.4	25.45
9	20.7	17.8	52	13.1	24.59	22.0	16.6	66	12.3	27.24
9	20.9	18.5	52	13.3	19.40	22.2	17.1	66	13.9	19.45
9	21.3	19.6	52	13.2	20.66	22.4	17.6	66	12.4	17.89
9	21.6	20.0	52	12.5	18.55	22.7	18.3	66	13.2	23.21
9	21.9	21.1	53	11.1	21.77	22.8	20.5	68	11.9	22.64
9	22.1	21.4	53	11.8	25.87	23.1	21.1	68	11.3	24.05
9	22.4	21.8	53	11.9	22.18	23.5	21.4	68	12.1	23.45
9	22.5	22.0	53	12.2	21.05	23.7	21.8	68	11.6	25.71
9	22.7	22.2	53	12.9	20.23	23.8	22.2	68	12.6	25.77
12	21.7	16.1	60	14.7	27.83	24.8	23.3	74	17.1	28.59
12	21.8	17.2	60	14.9	27.69	25.0	24.4	74	19.4	26.43
12	22.0	17.8	60	14.5	27.59	25.2	25.0	74	15.2	26.84

12	22.3	18.3	60	16.1	22.15	25.3	25.6	74	15.8	28.63
12	22.4	18.9	60	14.9	30.80	25.4	27.2	74	17.9	19.73
12	22.6	20.0	61	14.4	25.68	25.4	26.1	76	17.1	19.24
12	22.8	21.1	61	15.3	25.20	25.6	26.8	76	17.4	22.97
12	23.1	22.2	61	14.6	24.84	25.7	27.2	76	16.2	23.59
12	23.2	21.1	61	15.2	27.54	25.9	27.5	76	16.7	22.23
12	23.4	22.3	61	14.2	28.41	26.2	27.9	76	17.1	21.35
12	19.1	18.5	62	14.7	27.12	23.1	18.3	78	14.8	26.69
12	19.2	18.9	62	14.8	25.46	23.2	18.8	78	14.3	31.82
12	19.4	19.4	62	14.4	27.37	23.4	19.4	78	14.6	24.66
12	19.5	19.8	62	14.5	28.25	23.5	19.8	78	14.4	24.57
12	19.6	20.1	62	14.4	26.01	23.7	20.0	78	14.5	26.46

Table 2.3: Geyser data for A1 experiments (d = 3″, $d/D = 1/2$)

	S1 (V_w = 0.772 m^3, V_a = 0.918 m^3)					*S2* (V_w = 0.961 m^3, V_a = 0.729 m^3)				
H	T_w	T_a	P_a	t	h_g	T_w	T_a	P_a	t	h_g
(m)	(°C)	(°C)	(psi)	(s)	(m)	(°C)	(°C)	(psi)	(s)	(m)

3	18.7	17.2	34	55.9	1.82	20.9	16.2	44	28.7	2.00
3	18.8	16.8	34	52.3	1.88	20.8	16.0	44	50.3	1.32
3	19.0	16.4	34	33.5	2.00	20.7	15.3	44	36.6	1.54
3	19.3	17.2	35	37.3	2.06	20.3	13.9	45	32.8	1.80
3	19.3	17.5	35	28.1	1.97	20.0	13.4	45	35.7	2.29
3	19.4	17.8	35	41.8	1.23	19.7	12.5	45	29.3	1.36
3	19.5	17.6	37	26.6	2.74	19.6	12.0	45	28.1	2.84
3	19.5	17.4	37	30.4	2.89	20.7	16.1	47	24.9	3.39
3	19.7	17.2	37	26.6	3.13	20.7	15.5	47	27.0	2.46
6	21.1	22.8	43	25.2	8.13	25.4	23.1	53	20.1	8.68
6	21.2	23.7	43	27.1	8.81	25.8	22.1	53	19.1	8.24
6	21.3	24.2	43	24.4	6.13	26.2	21.1	53	18.1	7.95
6	21.6	24.7	43	25.2	7.93	26.3	20.6	53	17.5	8.79
6	21.7	25.0	43	29.4	6.57	26.4	20.1	53	20.8	10.22
6	18.1	12.2	44	26.1	13.62	26.7	21.0	55	12.1	8.66
6	18.1	13.1	44	20.8	11.65	26.8	19.7	55	10.1	11.46
6	18.2	14.2	44	28.2	11.47	27.0	19.4	55	14.7	8.68
6	18.3	16.5	44	25.8	11.21	26.9	19.3	55	11.3	9.37
6	18.4	17.0	44	20.1	10.60	26.9	19.0	55	11.2	7.34
6	18.5	17.2	45	18.5	10.69	26.8	19.1	57	8.6	9.32

6	18.7	17.6	45	20.5	10.29	26.3	18.5	57	9.2	11.77
6	18.7	17.9	45	20.5	9.76	26.0	18.0	57	9.6	11.54
6	18.8	18.5	45	18.1	11.99	25.9	17.8	57	9.1	13.11
6	18.9	18.9	45	18.2	13.90	25.7	17.3	57	8.9	14.15
9	17.8	16.2	51	29.5	13.88	18.3	16.5	64	29.4	15.87
9	17.9	15.5	51	34.1	13.92	18.4	17.8	64	28.3	16.41
9	19.0	15.0	51	35.7	13.10	20.7	20.1	64	23.6	18.23
9	19.1	16.9	51	25.2	11.82	20.8	20.4	64	24.7	13.46
9	19.2	17.2	51	26.1	17.41	18.4	18.3	66	23.7	16.92
9	19.4	14.0	52	25.5	12.05	18.6	19.2	66	25.5	16.52
9	19.6	13.6	52	25.1	14.49	18.6	20.0	66	24.8	17.66
9	19.9	12.8	52	26.1	17.60	21.0	20.9	66	23.7	11.81
9	19.3	17.8	52	26.3	13.48	21.1	21.6	66	21.9	18.58
9	19.5	18.3	52	24.8	15.86	22.3	22.5	68	22.1	22.92
9	19.8	13.9	53	26.2	16.60	19.1	22.2	68	22.1	19.24
9	20.0	14.0	53	28.5	16.89	21.3	21.7	68	23.7	17.79
9	19.8	18.7	53	25.6	15.16	21.9	21.9	68	24.8	19.71
12	18.4	16.1	60	34.2	19.37	20.2	12.2	74	39.4	17.40
12	18.3	16.3	60	27.6	17.66	20.5	12.7	74	32.7	15.99
12	18.2	16.5	60	29.3	18.39	18.9	14.4	74	30.4	19.31

12	18.0	17.2	61	29.1	17.72	18.9	14.3	74	33.3	17.22
12	17.8	17.0	61	30.9	21.77	18.8	14.0	74	34.2	13.72
12	17.7	16.8	61	31.3	20.84	18.5	14.7	76	28.6	21.07
12	17.2	17.2	62	31.7	23.48	18.2	15.0	76	32.4	21.39
12	20.8	21.1	62	28.4	21.30	18.1	14.4	76	30.9	19.32
12	20.9	21.4	62	28.7	20.12	18.1	12.8	78	28.8	18.91
12	21.1	21.8	62	28.7	20.76	17.8	12.5	78	31.6	18.62
12	21.1	22.2	62	30.2	21.16	17.6	12.2	78	32.8	22.82

Table 2.4: Geyser data for A2 experiments (d = 1.5″, $d/D = 1/4$)

	S1 (V_w = 0.772 m^3, V_a = 0.918 m^3)					*S2* (V_w = 0.961 m^3, V_a = 0.729 m^3)				
H	T_w	T_a	P_a	t	h_g	T_w	T_a	P_a	t	h_g
(m)	(°C)	(°C)	(psi)	(s)	(m)	(°C)	(°C)	(psi)	(s)	(m)
3	20.6	21.2	34	102.6	0.66	18.3	17.2	44	80.1	0.61
3	20.4	21.3	34	150.8	0.49	18.4	17.6	44	109.6	0.67
3	20.3	21.5	34	166.9	0.50	18.9	17.8	44	114.8	0.54
3	20.1	21.7	35	93.3	1.15	20.1	18.5	45	83.2	0.87

3	20.0	21.2	35	95.9	0.90	20.2	18.6	45	79.5	1.16
3	20.1	22.8	35	88.3	0.93	20.2	18.9	45	106.6	0.85
3	20.0	22.8	37	83.2	0.72	20.4	19.0	47	74.3	1.36
3	20.0	21.5	37	74.7	1.22	20.6	20.1	47	77.9	0.88
3	19.8	21.0	37	80.5	0.86	20.3	22.2	47	73.1	1.21
6	20.6	18.9	43	108.8	3.07	21.5	21.2	53	100.9	2.27
6	20.9	18.7	43	94.8	3.22	21.5	19.6	53	125.3	2.37
6	21.1	18.2	43	121.2	2.51	21.4	18.3	53	114.2	3.07
6	21.5	21.2	44	100.5	2.00	21.5	21.1	55	84.2	2.04
6	21.8	21.5	44	101.6	3.20	21.3	18.9	55	97.1	3.03
6	21.9	21.9	44	109.7	2.60	21.2	17.8	55	105.7	2.57
6	22.4	22.2	45	82.1	3.11	21.4	20.6	57	96.1	3.11
6	22.6	22.5	45	93.4	2.34	21.3	18.9	57	88.5	3.09
6	22.7	22.8	45	98.8	2.48	21.2	17.2	57	89.9	2.40
9	20.4	17.2	51	124.5	3.58	18.2	13.9	64	136.5	1.89
9	20.2	17.1	51	116.7	3.15	18.2	15.7	64	136.9	2.52
9	20.0	17.1	51	139.2	3.51	18.4	16.1	64	142.1	2.71
9	19.5	16.1	52	111.2	3.90	18.5	12.8	66	114.2	2.97
9	19.6	15.5	52	143.4	2.81	18.6	14.1	66	138.9	2.79
9	19.3	13.9	52	132.9	2.99	18.6	15.0	66	129.9	3.23

9	18.9	13.8	53	127.5	2.73	19.2	16.1	68	103.5	3.71
9	18.4	13.1	53	132.6	3.23	19.2	15.2	68	126.9	2.98
9	17.9	12.2	53	110.6	4.29	19.4	14.0	68	128.4	3.92
12	18.5	17.2	60	150.2	3.25	17.5	13.9	74	151.8	3.37
12	18.5	16.4	60	132.4	5.21	17.5	14.1	74	152.6	3.05
12	18.4	16.1	60	155.7	4.68	17.7	14.5	74	145.6	3.26
12	18.3	15.7	61	141.7	4.54	17.9	14.5	76	110.4	5.52
12	18.2	14.8	61	163.3	4.76	18.0	1.7	76	134.1	4.87
12	18.3	13.9	61	156.4	4.25	18.5	15.0	76	152.4	4.64
12	18.1	13.8	62	133.8	3.52	18.7	16.1	78	149.6	4.01
12	18.0	13.1	62	128.3	4.36	19.2	16.5	78	125.8	6.05
12	18.0	12.8	62	152.1	3.86	19.5	17.2	78	130.3	3.84

Table 2.5: Geyser data for A3 experiments (d = 0.75″, $d/D = 1/8$)

	S1 (V_w = 0.772 m^3, V_a = 0.918 m^3)					*S2* (V_w = 0.961 m^3, V_a = 0.729 m^3)				
H	T_w	T_a	P_a	t	h_g	T_w	T_a	P_a	t	h_g
(m)	(°C)	(°C)	(psi)	(s)	(m)	(°C)	(°C)	(psi)	(s)	(m)

3	21.2	23.8	34	513.8	0.43	22.5	21.1	44	593.7	0.20
3	21.2	23.6	34	618.1	0.39	22.5	20.4	44	467.4	0.40
3	21.0	23.2	34	530.2	0.50	22.4	20.0	44	566.4	0.53
3	20.8	22.8	35	466.5	0.61	22.4	17.2	45	501.3	0.42
3	20.6	22.6	35	520.3	0.32	22.4	17.5	45	446.2	0.35
3	20.6	22.5	35	597.2	0.47	22.3	17.8	45	501.6	0.59
3	20.1	22.0	37	485.1	0.95	22.2	17.8	47	449.4	0.65
3	20.0	21.9	37	414.1	0.76	22.1	17.6	47	472.0	0.81
3	20.1	21.7	37	462.8	0.52	22.2	17.2	47	434.3	0.47
6	18.7	17.7	43	956.5	1.24	22.2	23.2	53	891.1	0.80
6	18.8	13.4	43	880.6	0.76	19.1	14.9	53	700.1	1.05
6	19.0	12.7	43	858.1	1.58	22.3	24.1	53	782.1	0.86
6	19.1	13.0	43	812.2	0.73	19.4	16.5	53	699.8	0.85
6	19.0	16.8	43	774.1	0.99	22.5	25.3	53	759.9	0.93
6	20.1	15.2	44	847.7	0.17	19.5	17.2	55	997.1	0.85
6	20.0	14.3	44	714.3	1.14	19.6	17.5	55	855.1	0.76
6	20.0	15.7	44	810.1	0.90	19.6	17.8	55	724.7	1.53
6	19.9	16.2	44	914.7	0.70	19.8	18.5	55	995.7	0.75
6	19.8	17.1	44	962.1	0.72	19.9	19.8	55	717.7	1.51
6	18.6	14.1	45	762.9	1.26	19.9	20.0	57	708.3	1.58

6	18.7	15.2	45	965.4	1.44	20.1	21.1	57	811.0	0.81
6	18.5	13.3	45	812.9	1.75	20.3	22.2	57	878.8	1.17
6	18.5	13.7	45	715.2	1.18	20.3	22.7	57	714.4	1.56
6	18.4	13.2	45	703.6	0.97	20.5	23.0	57	882.9	1.23
9	23.2	22.7	51	938.3	1.32	21.6	17.8	64	1100.4	2.28
9	23.7	23.9	51	1053.4	2.20	22.2	18.0	64	991.3	2.28
9	24.0	25.0	51	1172.9	1.06	22.8	21.1	64	1078.2	1.87
9	24.2	27.0	52	880.5	3.71	23.0	22.2	66	909.6	1.63
9	24.4	27.2	52	895.5	1.98	23.5	22.8	66	1047.3	1.86
9	19.9	13.9	52	856.0	2.03	23.8	25.0	66	1070.7	2.55
9	20.5	15.0	53	928.4	1.66	24.1	25.4	68	808.6	1.40
9	20.9	15.4	53	981.7	2.27	24.7	26.5	68	864.7	2.58
9	23.5	25.8	53	898.2	2.72	25.2	27.2	68	778.6	2.97
12	27.4	28.9	60	1129.7	2.73	27.6	30.1	74	1235.8	3.09
12	27.2	27.8	60	1388.2	1.82	27.4	28.7	74	1119.5	2.09
12	27.2	27.2	60	1114.9	3.76	26.8	27.5	74	1027.6	1.92
12	27.0	27.5	61	1175.8	2.10	26.6	26.4	76	1044.1	2.49
12	26.9	28.5	61	1209.8	3.30	25.4	24.2	76	1158.3	2.36
12	26.9	30.0	61	989.5	2.76	25.3	24.1	76	1156.1	2.64
12	26.8	31.2	62	1062.0	2.26	23.5	24.5	78	1005.5	1.96

12	26.8	31.8	62	1141.5	2.35	23.8	26.1	78	1284.6	2.19
12	25.6	32.2	62	1179.1	2.62	24.1	26.5	78	1085.4	3.75

Chapter 3: Results and Discussion

3.1 Experimental Results of No-retrofitting Experiments

The data collected in the experiments (Table 2.2) have been analyzed based on the dimensional analysis discussed in a previous section. The plot of the dimensionless maximum eruption height and velocity as a function of the dimensionless air mass flow rate is shown in Figs. 3.1 and 3.2, respectively. As can be observed in these figures, in general, the larger is the dimensionless air mass flow rate, the larger is the geyser height and velocity. Figures 3.1 and 3.2 also show that the larger is the ratio H/D, the larger is the geyser height and velocity. The curve fitting for the dimensionless eruption height and velocity were performed based on Eqs. (3.3) and (3.4), respectively. These curve fittings are presented in Figs. 3.3 and 3.4, respectively. The 80% confidence bounds (if data distribution is approximately normal then 80% percent of the data values are within 1.28 standard deviations of the mean) are shown in the respective figures. The coefficients that fit best the data were obtained by the method of non-linear least squares. In the curve fittings, the values of $\alpha 2$ and $\alpha 3$ were very close to 0.5 and 1.0, respectively. Hence, the values of $\alpha 2$ and $\alpha 3$ were set to 0.5 and 1.0, respectively. Then, a new fitting was performed for $\alpha 1$ keeping constants $\alpha 2$ and $\alpha 3$. According to the dimensional analysis section, the fitting coefficients for the eruption velocity, $\beta 2$ and $\beta 3$, were obtained as $\beta 2 = \alpha 2/2$ and $\beta 3 = \alpha 3/2$.

The fitting coefficient $\beta 1$ was obtained by the method of non-linear least squares, which resulted in a value of 6.565. From the dimensional analysis section, $\beta 1 = \sqrt{2\alpha 1}$, which gives a value of 6.576, which in turn is close to the value obtained by the method of non-linear least squares (6.565). The resulting fitted equations for the dimensionless eruption height and velocity are given by

$$\frac{h_g}{D} = 21.621\left(\frac{\dot{M}}{\rho_w\sqrt{gD^5}}\right)^{0.5}\left(\frac{H}{D}\right) \tag{3.1}$$

$$\frac{w}{\sqrt{gD}} = 6.565\left(\frac{\dot{M}}{\rho_w\sqrt{gD^5}}\right)^{0.25}\left(\frac{H}{D}\right)^{0.5} \tag{3.2}$$

The goodness of fit in Eqs. (3.5) and (3.6) have an R^2 value of 0.92 and 0.93, respectively, which indicate a good fit to the data. Figures 3.3 and 3.4 confirm the good fit of the data for the dimensionless eruption height and velocity, respectively. It is worth mentioning that the standard deviation of the data for *Series 2* experiments is larger than that of *Series 1* (see Figs. 3.3 and 3.4). It is speculated that the reason for the latter is that the *Series 2* experiments used less air volume than those of *Series 1*, which resulted in a larger uncertainty of the air mass flow rate for *Series 2* experiments.

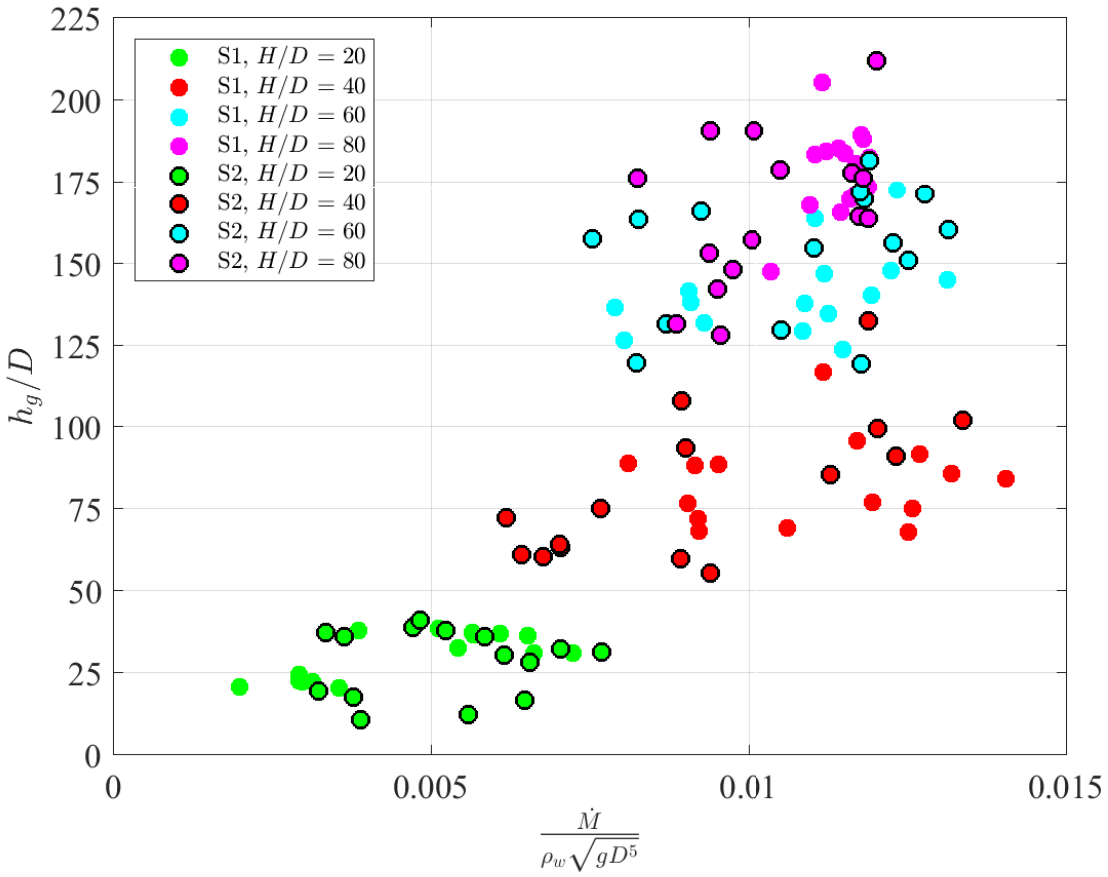

Figure 3.1: Dimensionless eruption height versus dimensionless air mass flow rate for no-retrofitting NR experiments

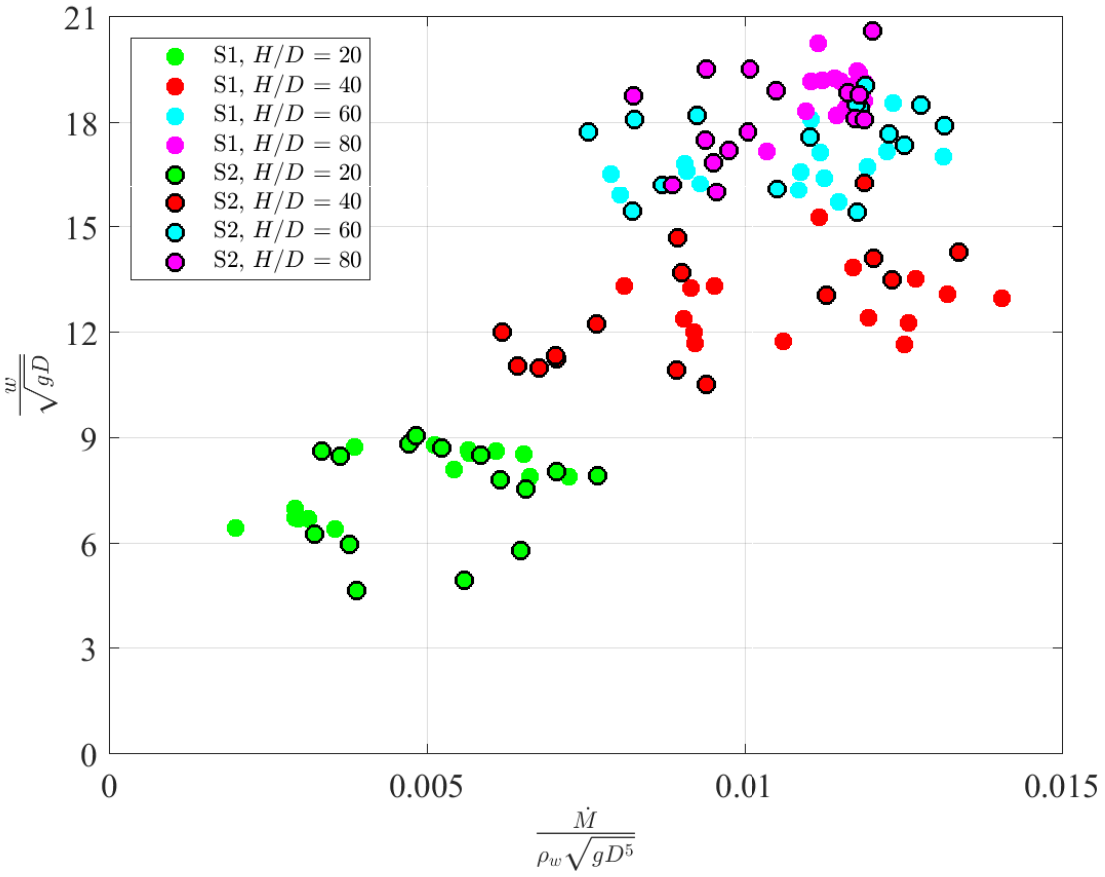

Figure 3.2: Dimensionless velocity versus dimensionless air mass flow rate for no-retrofitting NR experiments

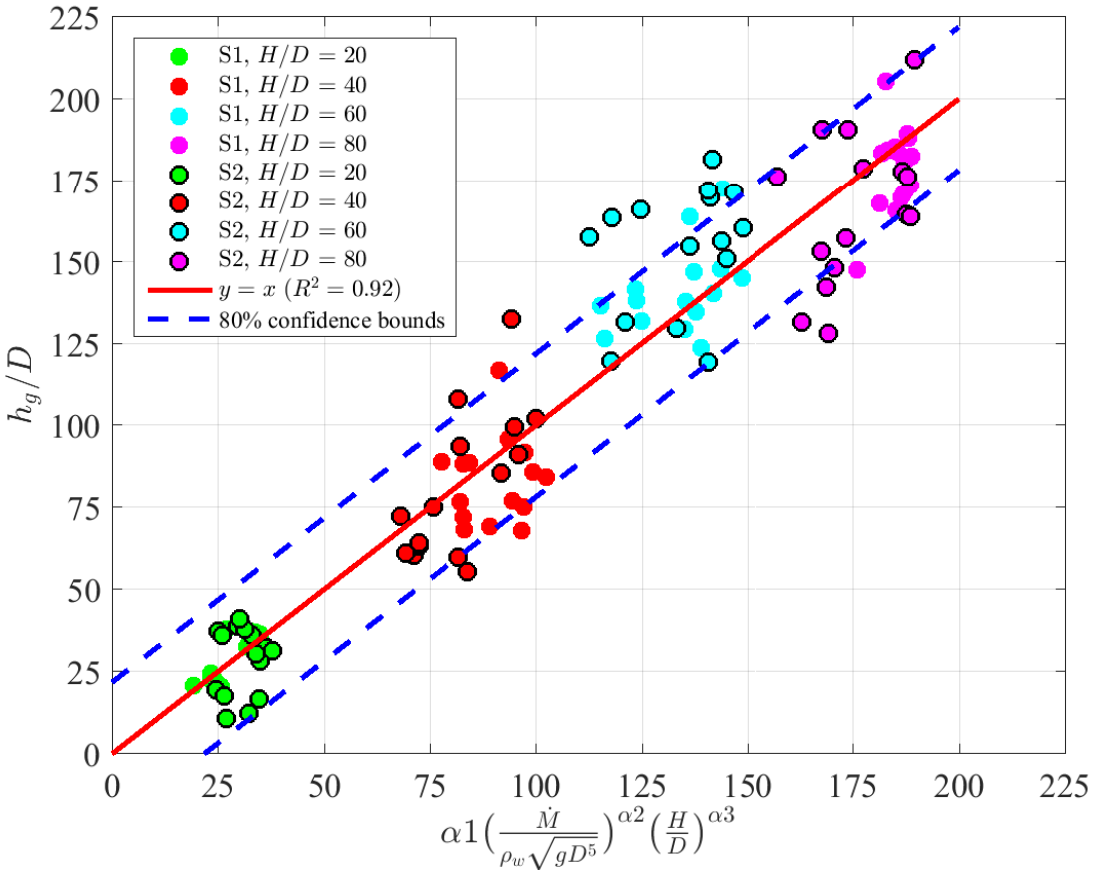

Figure 3.3: Curve fitting for dimensionless eruption height for no-retrofitting NR experiments ($\alpha 1$ = 21.621, $\alpha 2$ = 0.5 and $\alpha 3$ = 1.0)

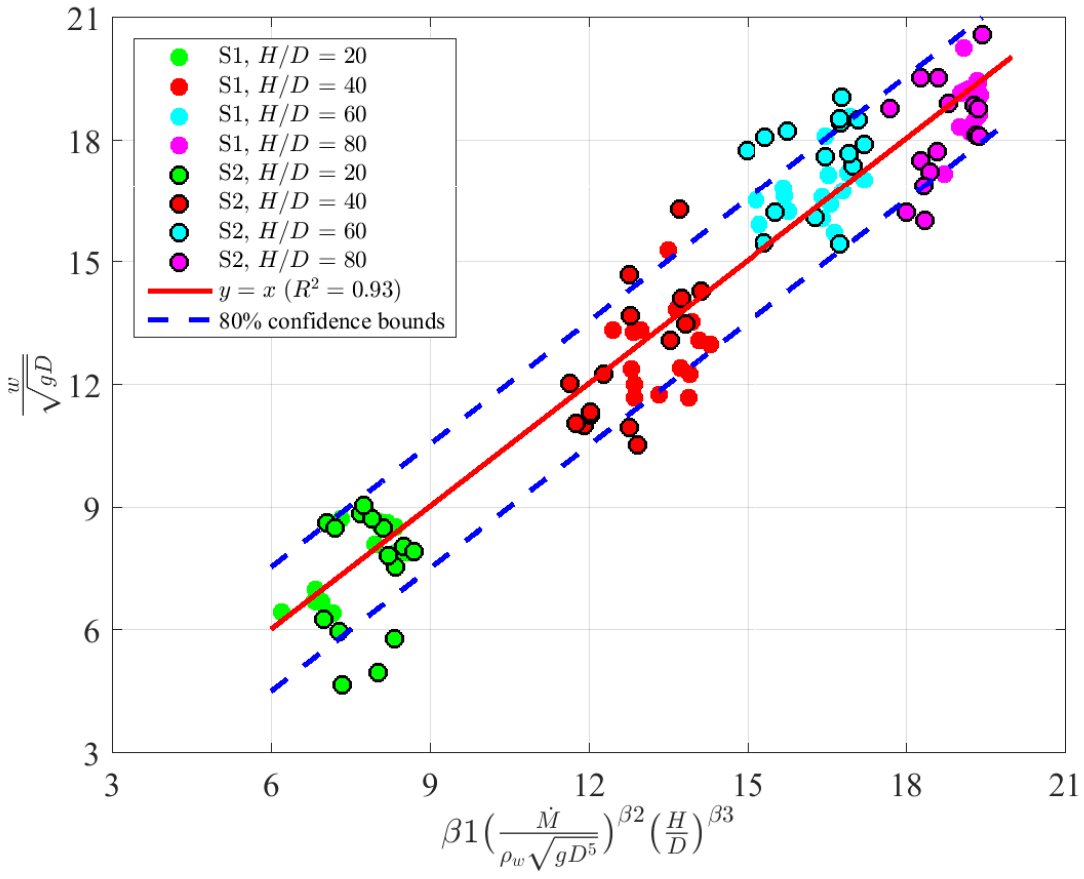

Figure 3.4: Curve fitting for dimensionless eruption velocity for no-retrofitting NR experiments ($\beta 1$ = 6.565, $\beta 2$ = 0.25 and $\beta 3$ = 0.5)

As mentioned earlier, the present laboratory experiments were performed using air as the gas. In addition to air that is entrapped in near-horizontal tunnels and that is transported to the dropshaft, it is argued that geysering is enhanced by exsolution of dissolved gases (e.g., [Leon, 2016a], [Leon, 2016c]). A sewer system contains a mixture of toxic and non-toxic gases that can be present at varying levels depending upon the source ([Hutter, 1993]). The gases

present in sewers include ammonia (NH_3), hydrochloric acid (HCl), hydrogen sulfide (H_2S), methane (CH_4), carbon dioxide (CO_2), carbon monoxide (CO), sulfur dioxide (SO_2) and chlorine (Cl_2) ([Viana et al., 2007], [Hutter, 1993]). For instance, ammonia, which is widely used in fertilizers, is present in large amounts in stormwater and combined sewer systems. Some of the gases, such as ammonia, are easily absorbed in water. [Ledig, 1924] has shown that ammonia is absorbed in water at least 100 times faster than carbon dioxide. In most cases, it is likely that dissolved gases are below saturation, however they can be exsolved when the air pocket moves bottom water upward to the point where dissolved gas pressure exceeds local hydrostatic pressure. The role of the exsolution of dissolved gases on the geyser intensity is not part of the present study.

3.2 Experimental Results of Retrofitting Methods

The data collected in the experiments (Tables 2.3 to 2.5) have been analyzed based on the dimensional analysis presented in a previous section. Because the retrofitting method (e.g., dropshaft diameter reduction) has a direct influence on the air mass flow rate, it is expected that the geyser height and velocity when considering the present retrofitting method can still be predicted using the same dimensionless relationships established for no-retrofitting experiments. The power

forms for the eruption height and velocity established in the companion paper are:

$$\frac{h_g}{D} = \alpha 1 \left(\frac{\dot{M}}{\rho_w \sqrt{g D^5}} \right)^{\alpha 2} \left(\frac{H}{D} \right)^{\alpha 3} \tag{3.3}$$

$$\frac{w}{\sqrt{gD}} = \beta 1 \left(\frac{\dot{M}}{\rho_w \sqrt{g D^5}} \right)^{\beta 2} \left(\frac{H}{D} \right)^{\beta 3} \tag{3.4}$$

The curve fitting for the dimensionless eruption height and velocity were performed based on Eqs. (3.3) and (3.4), respectively. In the curve fittings the values of $\alpha 2$, $\alpha 3$, $\beta 2$, and $\beta 3$ were fixed to the same values as those of the companion paper. This is justified because very close values to these coefficients are obtained when performing a curve fitting with no fixed coefficients. The curve fitting results for the retrofitting, no retrofitting, and combined cases are presented in Table 3.1. The respective goodness of fit are also shown in this Table. In a similar way to the geyser experiments with no retrofitting ([Leon et al., 2016]), the coefficients that fit best the data were obtained by the method of non-linear least squares. As can be observed in Table 3.1, the values of $\alpha 1$ and $\beta 1$ remain pretty much constant and in all cases the R^2 values are equal or higher than 0.89, which indicate a good fit to the data.

Because of the low variability of $\alpha 1$ and $\beta 1$, the coefficients for the combined case can be used as the general formula for predicting geyser height and velocity in presence or no presence of retrofitting. The resulting fitted equations for the combined case are given by

	Retrof.	No Retrof.	Combined
$\alpha 1$	20.347 R^2 = 0.89	21.621 R^2 = 0.92	21.165 R^2 = 0.93
$\beta 1$	6.018 R^2 = 0.89	6.565 R^2 = 0.93	6.297 R^2 = 0.92

Table 3.1: Fitting coefficients and the goodness of fit (R^2) for the retrofitting, non retrofitting, and combined cases

$$\frac{h_g}{D} = 21.165\left(\frac{\dot{M}}{\rho_w\sqrt{gD^5}}\right)^{0.5}\left(\frac{H}{D}\right) \tag{3.5}$$

$$\frac{w}{\sqrt{gD}} = 6.297\left(\frac{\dot{M}}{\rho_w\sqrt{gD^5}}\right)^{0.25}\left(\frac{H}{D}\right)^{0.5} \tag{3.6}$$

To verify that the retrofitting data has a good fit with Eqs. (3.5) and (3.6), Figs. 3.5 and 3.6 present the curve fittings for the dimensionless geyser height and velocity, respectively. These figures also present the 80% confidence bounds (if data distribution is approximately normal then 80% percent of the data values are within 1.28 standard deviations of the mean) and the goodness of fit (R^2). As can be observed in Figs. 3.5 and 3.6, the dimensionless eruption height and velocity for the retrofitting data have a good fit with the power forms in Eqs. (3.5) and (3.6), respectively.

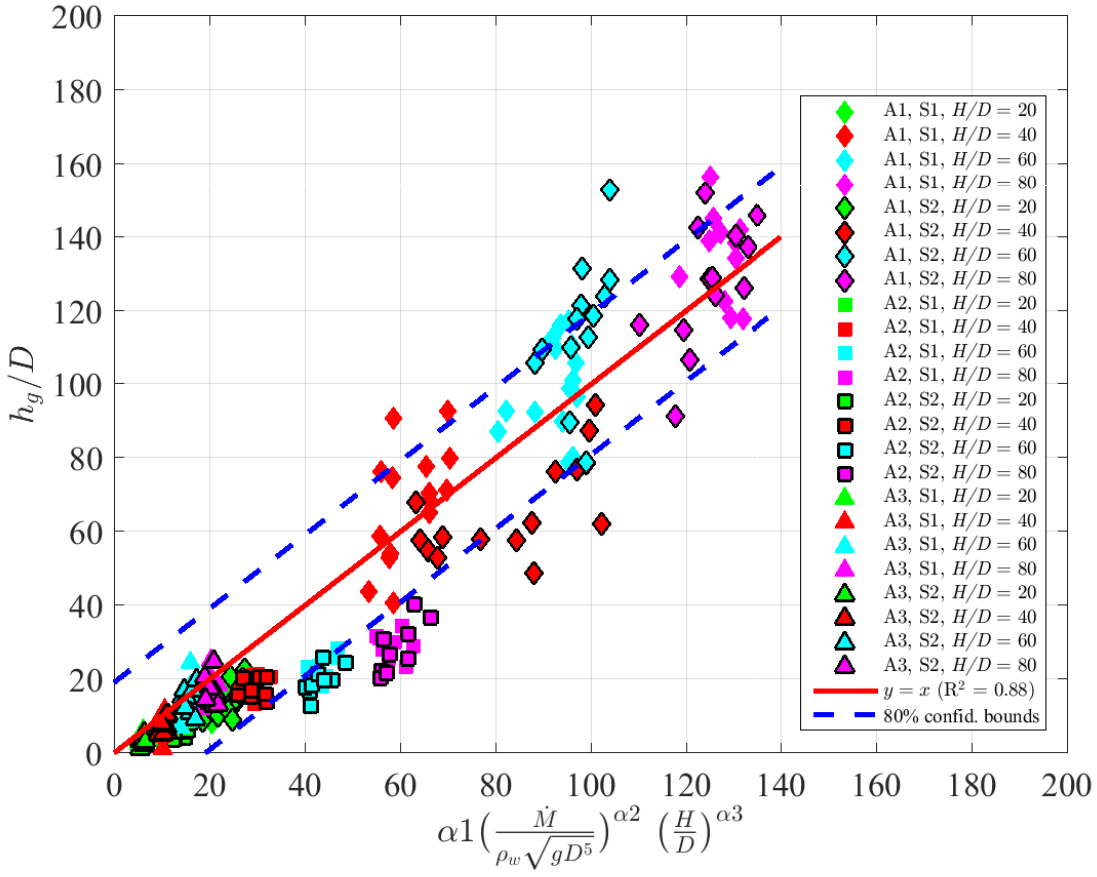

Figure 3.5: Curve fitting for dimensionless eruption height for retrofittings A1, A2 and A3 ($\alpha 1$ = 21.165, $\alpha 2$ = 0.5 and $\alpha 3$ = 1.0)

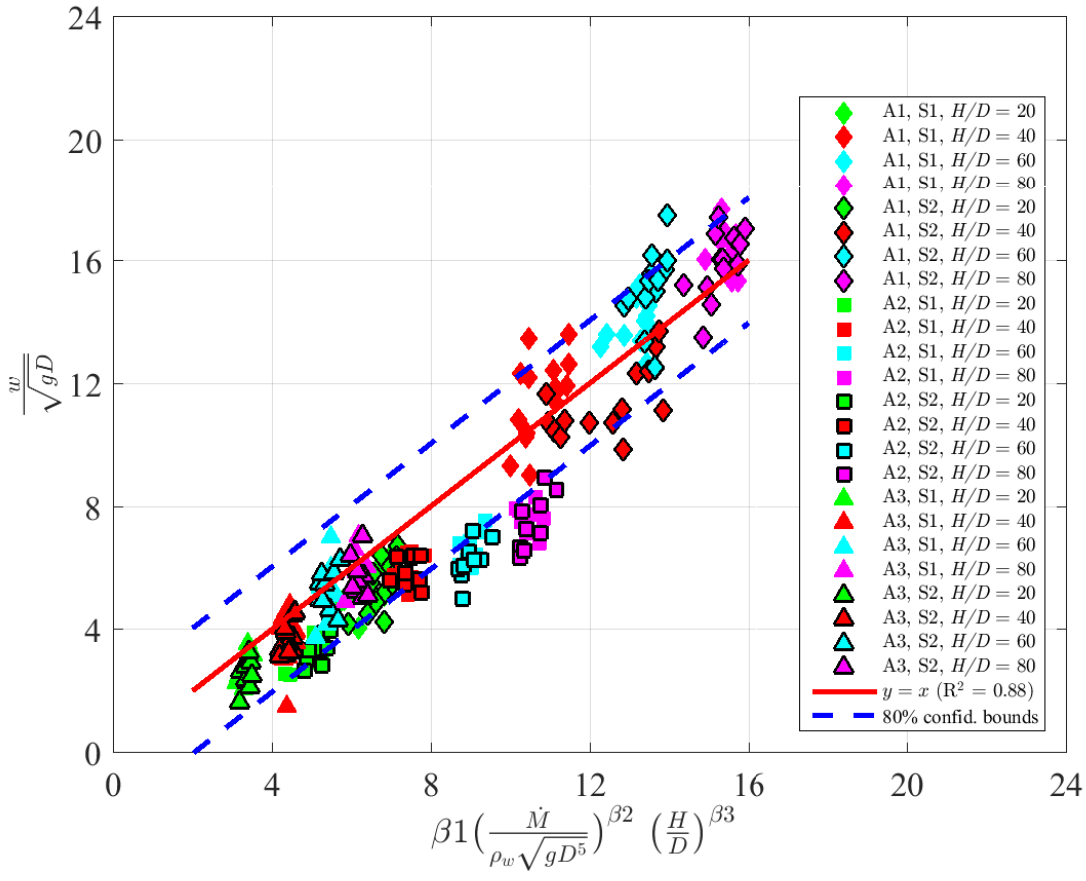

Figure 3.6: Curve fitting for dimensionless eruption velocity for retrofittings A1, A2 and A3 ($\beta 1$ = 6.297, $\beta 2$ = 0.25 and $\beta 3$ = 0.5)

3.3 Comparison of Experimental Results of No-retrofitting and Retrofitting Methods

To verify that the combined data (retrofitting and no retrofitting) have a good fit with Eqs. (3.5) and (3.6), Figs. 3.7 and 3.8 present the curve fittings for the dimensionless geyser height and

velocity, respectively. For clarity in the presentation of the combined data, the data of series 1 and series 2 for the retrofitting (A1, A2, A3) and non-retrofitting (NR) cases are combined. As can be observed in Figures 3.7 and 3.8, the geyser height and velocity for retrofitting A1 (d = 3″, d/D = 1/2) are not much smaller than those without retrofitting. The latter is because the area of the orifice for retrofitting A1 (25% of the cross-sectional area of the dropshaft) and the cross-sectional area of the initial air flow ($\approx 10 - 30\%$ of the cross-sectional area of the dropshaft) in the horizontal pipe have similar magnitude and hence there is no much restriction on the air mass flow rate. The geyser height and velocity for retrofittings A2 (d = 1.5″, d/D = 1/4) and A3 (d = 0.75″, d/D = 1/8) are much smaller than those without retrofitting. Figures 3.7 and 3.8 also show that the geyser height and velocity are relatively small for retrofitting A3 (d/D = 1/8).

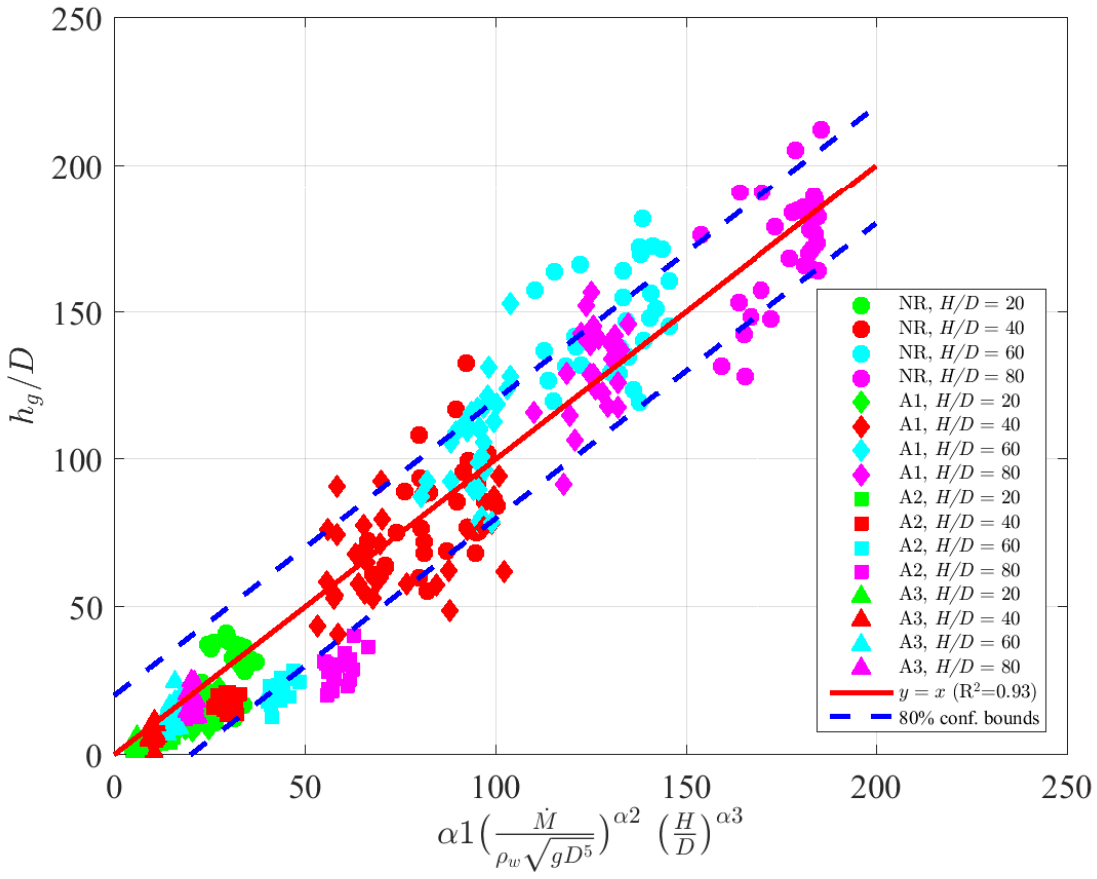

Figure 3.7: Curve fitting for dimensionless eruption height for retrofitting A1-A3 and no-retrofitting NR of the geyser experiments ($\alpha 1$ = 21.165, $\alpha 2$ = 0.5 and $\alpha 3$ = 1.0)

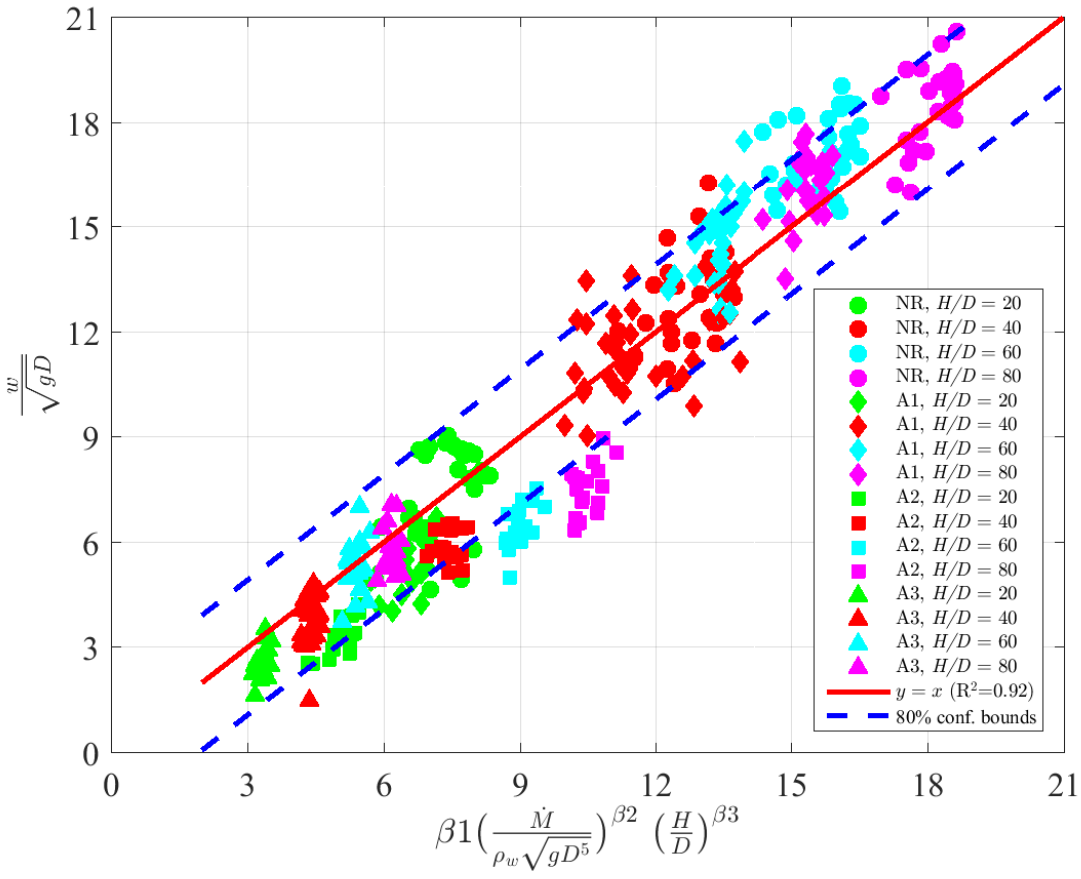

Figure 3.8: Curve fitting for dimensionless eruption velocity for retrofitting A1-A3 and no-retrofitting NR of the geyser experiments ($\beta 1$ = 6.297, $\beta 2$ = 0.25 and $\beta 3$ = 0.5)

Finally, Figures 3.9 and 3.10 present the combined data (retrofitting and no retrofitting) for the dimensionless eruption height and velocity as a function of the dimensionless air mass flow rate, respectively. As can be observed in these figures, in general, the smaller is the orifice diameter, the smaller is the air mass flow rate and the smaller is the geyser height and velocity. Figures 3.9 and 3.10 also show that the larger is the ratio H/D, the larger is the geyser height

and velocity.

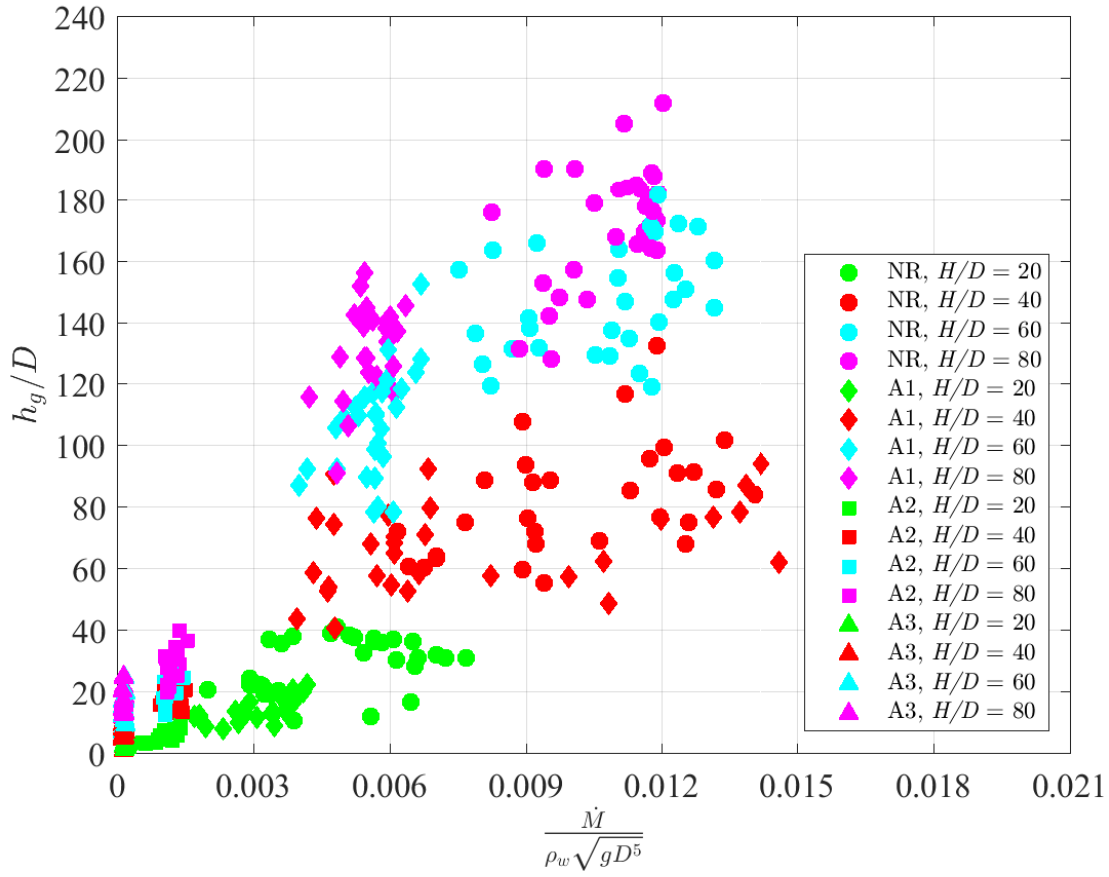

Figure 3.9: Dimensionless eruption height versus dimensionless air mass flow rate for retrofitting A1-A3 and no-retrofitting NR of the geyser experiments

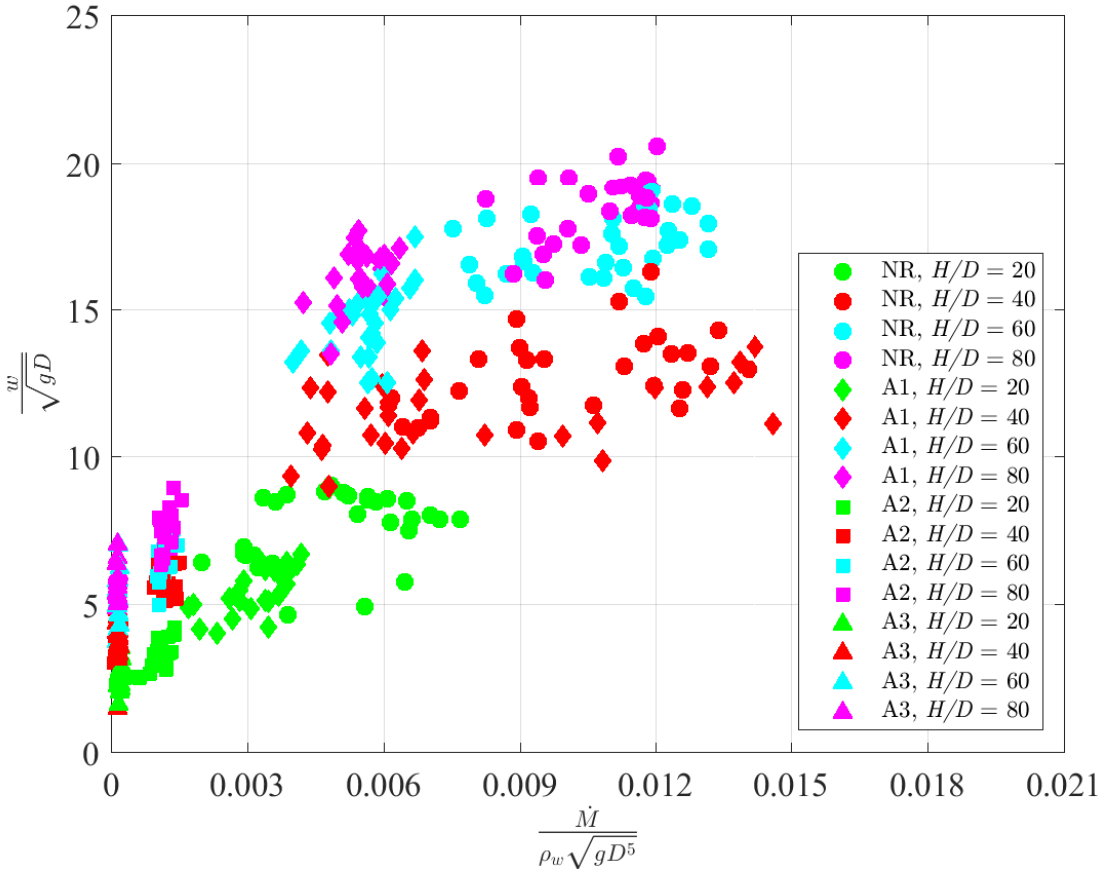

Figure 3.10: Dimensionless velocity versus dimensionless air mass flow rate for retrofitting A1-A3 and no-retrofitting NR of the geyser experiments

Chapter 4: Conclusion

This thesis presents an experimental study on violent geysers in vertical shafts and a retrofitting method to minimize geyser intensity. The key results are as follows:

1. The present research has produced for the first time violent geysers in a laboratory setting. The geysers produced consist of a few consecutive eruptions within a time frame of a couple of seconds with heights that may exceed 30 m. These characteristics resemble those of geysers that occurred in actual stormwater and combined sewer systems.

2. This research resulted in dimensionless relationships to predict eruption height and velocity in vertical shafts.

3. The dimensionless eruption height and velocity were found to have a good fit with the power forms obtained in the dimensional analysis.

4. The eruption height and velocity were found to increase with the dimensionless air mass flow rate and the ratio H/D, where H is the dropshaft height and D is the dropshaft diameter.

5. The eruption height and velocity were found to decrease with a decrease of the orifice diameter (e.g., lower air mass flow rate) and a decrease of H/D, where H is the dropshaft

height and D is the dropshaft diameter. In general, the smaller is the orifice diameter, the smaller is the air mass flow rate and the smaller is the geyser height and velocity.

6. The dimensionless eruption height and velocity were found to have a good fit with the power forms obtained in the dimensional analysis.

7. The proposed retrofitting method was found to be an effective strategy for minimizing the intensity of violent geysers in vertical shafts. For the experimental conditions considered in the present study, a geyser eruption is nearly eliminated when d/D is about 1/8, where d is the orifice diameter.

Bibliography

[EPA, 2004] EPA (2004). Impacts and Control of CSOs and SSOs. Report to Congress EPA 833-R-04-001, United States Environmental Protection Agency, Office of Water (4203), Washington, D.C. 20460.

[Guo and Song, 1991] Guo, Q. and Song, C. S. S. (1991). Hydrodynamics under transient conditions. *J. Hydraul. Eng*, 117(8):1042–1055.

[Hamam and McCorquodale, 1982] Hamam, M. A. and McCorquodale, J. A. (1982). Transient conditions in the transition from gravity to surcharged sewer flow. *Can. J. Civ. Eng.*, 9.

[Hutter, 1993] Hutter, G. M. (1993). Reference data sheet on sewer gas(es).

[Ledig, 1924] Ledig, P. G. (1924). Absorption of carbon dioxide and ammonia from gas bubbles. *Industrial & Engineering Chemistry*, 16(12):1231–1233.

[Leon, 2006] Leon, A. S. (2006). *Improved modeling of unsteady free Surface, pressurized and mixed Flows in storm-sewer systems*. PhD thesis, Univ. of Illinois at Urbana-Champaign, Urbana, IL.

[Leon, 2016a] Leon, A. S. (2016a). Mathematical models for quantifying eruption velocity in degassing pipes based on exsolution of a single gas and simultaneous exsolution of multiple gases. *J. volcanology and geothermal research*, 323(1):72–79.

[Leon, 2016b] Leon, A. S. (2016b). Mechanisms that lead to violent geysers in stormwater and combined sewer systems and a simplified model for estimating geyser velocity in these systems. *Journal of Hydraulic Research (under review)*.

[Leon, 2016c] Leon, A. S. (2016c). Mechanisms that lead to violent geysers in stormwater and combined sewer systems and a simplified model for estimating geyser velocity in these systems. *Journal of Hydraulic Research (under review)*.

[Leon et al., 2016] Leon, A. S., Elayeb, I., and Tang, Y. (2016). An experimental study on violent geysers in vertical shafts: Part I – No retrofitting. *Journal of Hydraulic Engineering (under review)*.

[Leon et al., 2006] Leon, A. S., Ghidaoui, M. S., Schmidt, A. R., and García, M. H. (2006). Godunov-type solutions for transient flows in sewers. *Journal of Hydraulic Engineering*, 132(8):800–813.

[Leon et al., 2010] Leon, A. S., Ghidaoui, M. S., Schmidt, A. R., and García, M. H. (2010). A robust two-equation model for transient mixed flows. *Journal of Hydraulic Research,*, 48(1):44–56.

[Lewis, 2011] Lewis, J. M. (2011). *A Physical Investigation of Air/Water Interactions Leading to Geyser Events in Rapid Filling Pipelines*. PhD thesis, University of Michigan.

[Pfister and Chanson, 2014] Pfister, M. and Chanson, H. (2014). Two-phase air-water flows: Scale effects in physical modeling. *Journal of Hydrodynamics, Ser. B*, 26(2):291 – 298.

[Vasconcelos, 2005] Vasconcelos, J. G. (2005). *Dynamic Approach to the description of flow regime transition in stormwater systems*. PhD thesis, University of Michigan.

[Viana et al., 2007] Viana, P., Yin, K., Zhao, X., and Rockne, K. (2007). Modeling and control of gas ebullition in capped sediments. In *Proceedings of the 4th International Conference on Remediation of Contaminated Sediments*, pages 22–25, Columbus, OH, USA. Battelle Press.

[Wright et al., 2011] Wright, S. J., Lewis, J. W., and Vasconcelos, J. G. (2011). Geysering in rapidly filling storm-water tunnels. *J. Hydraul. Eng*, 137(1):112–115.